Catal Lett (2012) 142:1075–1081
DOI 10.1007/s10562-012-0868-3

Synthesis of a Novel Nano-Sized Pt/ZnO Catalyst for Water Gas Shift Reaction in Medium Temperature Application

Vijayanand Subramanian · Hari S. Potdar · Dae-Woon Jeong · Jae-Oh Shim · Won-Jun Jang · Hyun-Seog Roh · Un Ho Jung · Wang Lai Yoon

Received: 3 May 2012 / Accepted: 2 July 2012 / Published online: 19 July 2012

Abstract A novel nano-sized Pt/ZnO catalyst has been prepared by impregnating 1 wt% Pt on a nano-sized ZnO supports, with spherical and rod-type morphology and tested for the water gas shift reaction at a gas hourly space velocity of 9,583 h^{-1}. The Pt/ZnO catalyst with spherical ZnO morphology exhibited an almost thermodynamic equilibrium CO conversion value of 70 % at 400 °C with 100 % CO_2 selectivity. The high activity/stability of the catalyst is due to a good interfacial contact between Pt and ZnO.

Keywords Pt/ZnO catalyst · Water gas shift reaction · Medium temperature

1 Introduction

Generation of pure H_2 streams has become quite important in the last decade because modern hydrogen-based fuel cells appear to be one of the most promising environmentally friendly substitutes for gas-oil and biodiesel vehicle fuels [1–3]. Recently, nearly 95 % of the H_2 used in industry is generated essentially from hydrocarbons (HCs) [4]. The synthesis gas (CO + H_2) produced from reforming of HCs can contain up to 10 % of CO, which should be removed for the fuel cell application [5]. In this respect, the water gas shift reaction (WGS: CO + $H_2O \rightarrow H_2 + CO_2$) constitutes a critical process for on-site generation and purification of H_2. Consequently, a hydrogen fuel economy requires improved air-tolerant, cost effective WGS catalysts for lower and medium temperature processing, allowing mobile fuel cell applications under cyclic and stationary conditions [2, 6, 7]. Recent review article published by Baronskaya et al. [8] gives an elaborate survey of the present state of the art regarding advanced WGS catalysts and also emphasizes a need to develop a highly active WGS catalyst in a wide temperature window. This can be possibly done either by suitably modifying existing traditional catalyst compositions or alternatively designing and synthesizing nano-sized based catalysts with new chemical compositions. Many recent experimental and theoretical studies have addressed this particular aspect/topic in details, and suggested to replace catalysts based on Fe_2O_3/Cr_2O_3 and $Cu/ZnO/Al_2O_3$ oxides delineating the problems associated with them [9–13]. Some problems associated with traditional WGS catalysts were solved by loading 1–5 wt% of Pt, Cu, Au and bimetallic nano-sized particles on reducible (TiO_2, CeO_2, $Ce–ZrO_2$) and irreducible supports (Al_2O_3, SiO_2), respectively [14–19]. It is well established that the activity/stability of these catalysts in WGS can be tailored by controlling not only physical/chemical characteristics of metals as well as supports but also by their interactions [20]. It has been postulated that the bi-functional mechanism can be operative where the Pt sites adsorbed CO, and sites on the support or at metal–support interface decomposed H_2O providing oxygen for reaction with CO [21]. For the partially reducible supports, Pt promotes the reduction of support such that bridging OH group is formed, which reacts with CO to form the associative species such as formates. Further with the aid of the Pt at the metal support

V. Subramanian · H. S. Potdar · D.-W. Jeong · J.-O. Shim · W.-J. Jang · H.-S. Roh (✉)
Department of Environmental Engineering, Yonsei University, 1 Yonseidae-gil, Wonju, Gangwon 220-710, Republic of Korea
e-mail: hsroh@yonsei.ac.kr

U. H. Jung · W. L. Yoon (✉)
Hydrogen Energy Research Center, Korea Institute of Energy Research (KIER), 71-2 Jang-dong, Yuseong-gu, Daejeon 305-343, Republic of Korea
e-mail: wlyoon@kier.re.kr

interface, these species dehydrogenate at low temperature. [22, 23]. Pt metal helps to enhance the reducibility of the support, thus promoting the water activation step. The extensive investigation made by Pigos et al. [24, 25] showed the addition of alkali promotes the formation of OH groups that react with CO to produce intermediates like formates that decompose readily at the metal oxide interface due to the weakening of bond associated intermediate with hydrogen. Oxidized Pt species (PtO_x) are known to be active species for WGS [20]. Zhai et al. [19] showed that the partially oxidized Pt–Na–$O_x(OH)_y$ species are the active sites for WGS, which can be stabilized by adding alkali ions to irreducible supports like alumina or silica supports.

Cu, Au, and Pd supported on ZnO catalysts are applied for various important reactions such as selective hydrogenation of CO_2 to methanol, selective oxidation of CO in the presence of hydrogen, steam reforming of methanol to produce synthesis gas and dehydrogenation of isobutane to isobutene [26–30]. Also, Pt/ZnO catalysts have been tried especially under reducing conditions in selective hydrogenation of crotonaldehyde to crotyl alcohol [31, 32]. In these catalysts, the interaction of Pt with partially reduced ZnO supports or even with Zn metal particles, formed at the interface under reducing conditions in the absence of steam is exploited to improve the selectivity by an increase in electron density of the Pt. On the contrary, we planned to create an oxidizing environment by using steam, which can effectively re-oxidize the partially reduced ZnO support or even fine PtZn alloy particles formed at the interface and lower the electron density of the Pt, and hence to stabilize Pt in the form of PtO_x, species, which are known to be active species for WGS. Also Shido et al. [33] have demonstrated the formate mechanism occurs on ZnO. Partial reduction of the oxide is required in order to facilitate the dissociation of H_2O on the oxide surface, so that the formate species can be formed by the reaction of these special Type II bridging OH groups with CO [34]. Since the partial reduction of the oxide occurs at lower temperature, the formates are readily generated at lower temperatures. In addition, it has been known that the formate decomposition rate is also significantly accelerated, since the noble metal can facilitate abstraction of hydrogen at the metal oxide interface [22, 23]. It is likely, therefore, that an analog would exist for ZnO, whereby addition of Pt should also promote formate formation at low temperature, and also accelerate its decomposition. Therefore, an attempt is made to demonstrate this particular concept by using the nano-sized Pt/ZnO catalyst in catalyzing WGS. The objective of the present work is to synthesize nano-sized Pt/ZnO catalysts with different morphology, and demonstrate their ability in catalyzing WGS in the medium temperature range. Two Pt catalysts supported on spherical or rod-type ZnO supports, prepared by varying the synthesis conditions, are subjected to the activity study in order to develop a correlation based on morphological features. All these results related to synthesis, characterization and testing of nano-sized Pt/ZnO catalysts in WGS are reported in this paper.

2 Experimental

2.1 Synthesis of ZnO Support and Pt/ZnO Catalyst

Equal volumes of solution containing $Zn(NO_3)_2{\cdot}6H_2O$ (0.05 M) and K_2CO_3 (0.08 M) are added drop by drop from separate burettes to a well stirred 200 ml de-ionized water at room temperature (RT) to precipitate zinc hydroxy carbonate (ZHC) precursor particles at the pH of 8.0. The precursor particles are digested at RT for 8 h (ZRT). The same procedure was followed to prepare another sample (Z70) by keeping all the conditions same except the temperature kept at 70 °C instead of RT. The crystalline ZHC precursors were thoroughly washed with de-ionized water several times to avoid K^+ ions contamination and further dried in oven at 70 °C over night. Then crystalline ZnO supports were obtained by the controlled decomposition of as-dried ZHC precursors (ZRT and Z70) at 300 °C for 3 h in air and named as ZRT-300 and Z70-300. 1 wt% Pt/ZnO catalysts were prepared by an incipient wetness impregnation method using $Pt(NH_3)_4(NO_3)_2$ (99 %, Aldrich). The final catalysts Pt/ZRT-300 and Pt/Z70-300 were obtained by re-calcination of 1 wt% Pt loaded ZRT-300 and Z70-300 supports at 300 °C for 3 h in air.

2.2 Characterization

The BET surface area was measured by nitrogen adsorption at −196 °C using an ASAP 2010 (Micromeritics). The XRD patterns were recorded using a Rigaku D/MAX–IIIC diffractometer (Ni filtered Cu–Kα radiation, 40 kV, 50 mA). TGA study on the as-dried ZHC precursor from RT to 600 °C in air was carried out using a NETZSCH Thermogravimetry Analyzer (TG209F3) with a heating rate of 10 °C/min to decide the calcination temperature to obtain nano-sized ZnO support. High resolution transmission electron microscopy (HR–TEM) images were taken using a SEI, PECNAI G^2TF30 transmission electron microscopy. Temperature programmed reduction (TPR) experiments were carried out in a BEL–CAT (BEL Japan Inc.). Typically, 0.1 g of pre-calcined sample was loaded into a quartz reactor. The TPR experiments were performed using 10 % H_2 in Ar with a heating rate of 10 °C/min from 20 to 600 °C. The sensitivity of the detector was calibrated by reducing known weight of NiO. H_2 pulse chemisorption experiments were performed to determine Pt dispersion as described in our earlier paper [35].

2.3 Catalytic Reaction

Activity tests were carried out from 240 to 400 °C under atmospheric pressure in a fixed-bed micro-tubular quartz reactor with an inner diameter of 4 mm. The catalyst charge was 0.136 g. A thermocouple was inserted into the catalyst bed to measure the reaction temperature. Prior to each catalytic measurement, the catalyst was reduced in 5 % H_2/N_2 from RT to 300 °C at a heating rate of 3.3 °C/min and the temperature was maintained for 1 h. Afterwards, the temperature was decreased to 240 °C. The reactant gas stream consisted of 6.5 vol% CO, 7.1 vol% CO_2, 0.7 vol% CH_4, 42.4 vol% H_2, 28.7 vol% H_2O, and 14.5 vol% N_2. The feed $H_2O/(CH_4 + CO + CO_2)$ ratio was intentionally fixed at 2.0 due to the fact that a H_2O/CH_4 ratio is typically 3.0 in steam reforming of methane (SRM: $H_2O + CH_4 = 3H_2 + CO$) to avoid coke formation [36–45]. A gas hourly space velocity (GHSV) of 9583, 13652 and 45625 h^{-1} were employed to test the catalyst. Water was fed using a syringe pump and was vaporized at 150 °C upstream of the reactor. The reformed gas was chilled, passed through a trap to condense the residual water, and then allowed to flow to the on-line micro-gas chromatograph (Agilent 3000).

3 Results and Discussion

3.1 Synthesis of ZHC Precursor and ZnO Support

ZHC precursor can be synthesized by the following reaction (1):

$$5Zn(NO_3)_2 + 5K_2CO_3 + 6H_2O \rightarrow Zn_5(OH)_6(CO_3)_2\downarrow + 10KNO_3 + 3H_2O + 3CO_2\uparrow \quad (1)$$

The XRD pattern of as-dried precursor Z70 and ZRT are shown in Fig. 1. It shows all reflections of a ZHC phase [46]. It is evident that the Z70 sample indicates improved crystallinity compared to the ZRT sample. The TGA curve of an as-dried precursor (ZRT) is depicted in Fig. 2. It shows single step decomposition in air, leading to the formation of ZnO support by a reaction (2). The observed weight loss is found to be 26.3 %. The theoretical weight loss (26.0 %) calculated from a reaction (2) is consistent with an experimental weight loss of 26.3 %, indicating the formation of ZnO support.

$$Zn_5(OH)_6(CO_3)_2 \rightarrow 5ZnO + 2CO_2 + 3H_2O \quad (2)$$

Thus, TGA study indicates that an as-dried precursor formed by the reaction (1) has a composition of $Zn_5(OH)_6(CO_3)_2$, and the minimum calcination temperature; T ~300 °C is required to get ZnO support.

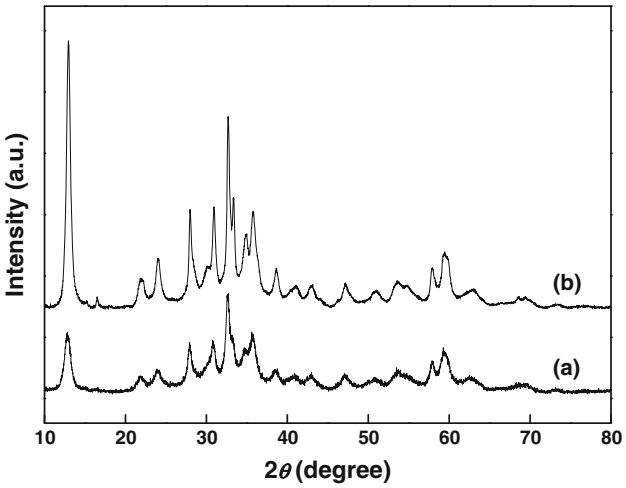

Fig. 1 XRD pattern of as-dried $Zn_5(CO_3)_2(OH)_6$ precursors (*a*) ZRT, (*b*) Z70

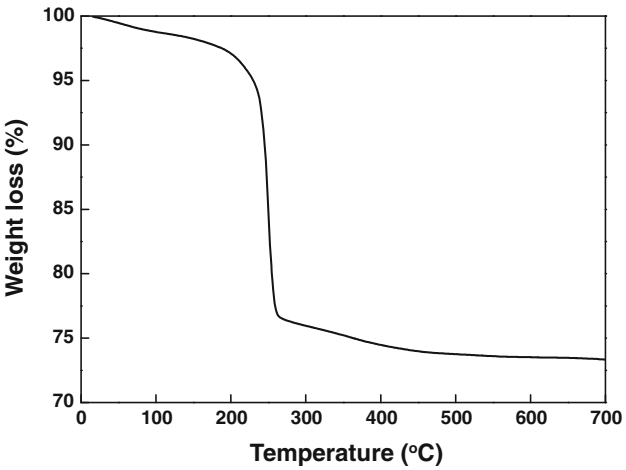

Fig. 2 TGA curve of as-dried $Zn_5(CO_3)_2(OH)_6$ precursor (ZRT)

Figure 3 shows XRD patterns of Z70-300, ZRT-300, and Pt/ZRT-300, respectively. In the case of support, all peaks are indexed to a ZnO phase with a hexagonal crystal structure [47]. The crystallite size was determined by using a Scherrer equation [48]. The crystallite sizes of Z70-300 and ZRT-300 are found to be 22.2 and 12.6 nm. Pt/ZRT-300 catalyst also shows peaks corresponding to a ZnO phase. The crystallite size of the ZnO support in Pt/ZRT-300 catalyst is 12.4 nm, which is almost the same as that of the pre-calcined ZnO support (ZRT-300), before impregnation of Pt. The peak reflections corresponding to Pt metal particles and oxidized (Zn–PtO_x) species do not appear. This indicates that the Pt metal particles or Zn–PtO_x species are finely dispersed on the nano-sized ZnO support.

The morphological features of the samples, as analyzed by HR–TEM, are shown in Fig. 4. It is interesting to note

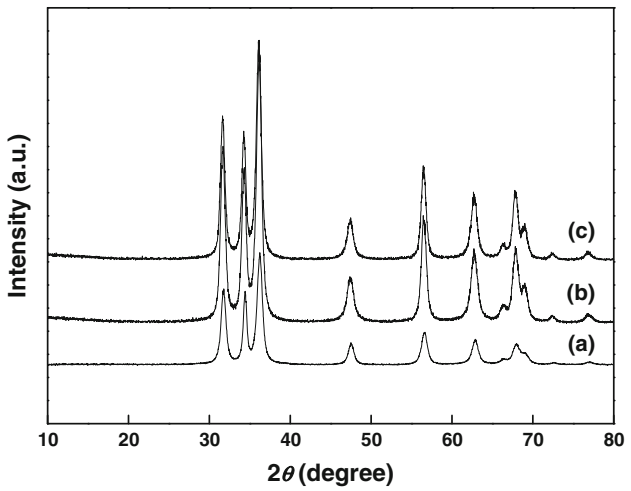

Fig. 3 XRD patterns of (*a*) Z70-300, (*b*) ZRT-300 and (*c*) Pt/ZRT-300

that the sample Z70-300 is rod-type. On the contrary, the sample synthesized at RT is spherical-type. In general, basic carbonates are known to retain their shape even after decomposition to their corresponding oxides [49]. Digestion carried out at higher temperature favors the formation of rods during the decomposition of basic zinc hydroxyl carbonate [50]. Also, it is clearly evident from the present case that two kinds of morphology are obtained by the variation in the digestion temperature during the synthesis.

The BET surface areas of Z70-300 and ZRT-300 are 68.0 and 46.6 m^2/g, respectively. Those values are comparable with that of reported ZnO support, prepared by urea method [51]. The BET surface area of the nano-sized Pt/ZRT-300 catalyst is 44.2 m^2/g, which is slightly lower than that of the pre-calcined ZnO support (ZRT-300) (46.6 m^2/g). This observation indicates that the ZnO support did not get sintered significantly during the re-calcination at 300 °C for 3 h in air. According to the H_2 chemisorption data, Pt dispersion and Pt surface area for Pt/Z70-300, Pt/ZRT-300 are 73.0, 77.3 % and 1.8, 1.9 m^2/g, respectively. Interestingly, though the surface area of Z70-300 is higher than ZRT-300, the Pt dispersion value is less. In both catalysts, the crystallite size of Pt is 1.5 nm, confirming the nano-sized nature of Pt particles. The homogeneous uniform interaction between the acidic Pt precursor solution and basic nature of ZnO support helps to form well dispersed nano-sized PtO_x particles during the re-calcination process in air. To evaluate the effect of Pt on the reducibility of the ZnO support, and to understand the nature of active species on the surface of catalyst, TPR study on both the ZnO support (ZRT-300) and Pt/ZnO catalyst (Pt/ZRT-300 and Pt/Z70-300) was performed. Figure 5 shows TPR profiles of the bare ZnO support (ZRT-300) and Pt/ZRT-300, Pt/Z70-300 catalysts. Figure 5a shows two broad reduction peaks. The first reduction peak at 307 °C can be attributed to the reduction of OH species associated with the ZnO support. The second broad reduction peak around 474 °C can be assigned to the reduction of surface oxygen from the ZnO support [52]. Chin et al. [28] also noticed a small amount of H_2 consumption between 280–500 °C. It was assigned to the partial reduction of ZnO at elevated temperature or surface reaction of pre-adsorbed species. On the contrary, Pt/ZRT-300 catalyst shows a sharp reduction peak at 150 °C and the second very weak peak around 460 °C. The first peak can be assigned to the reduction of oxidized Zn–PtO_x species, which are formed by the strong metal to support interaction (SMSI), together with a part of oxygen from the surface of ZnO support in close contact with Pt particles. The OH species associated with the ZnO support is possibly responsible for the formation of Zn–PtO_x species [53]. The second very weak reduction peak appearing about 460 °C is attributable to a sub-layer removal of oxygen from the ZnO support. In the case of Pt/Z70-300, the first peak appearing at 116 °C is due to the reduction of PtO_2 species, which have weak interaction with the support [54, 55]. However, the intensity of the peak appearing at 150 °C is weak. This observation

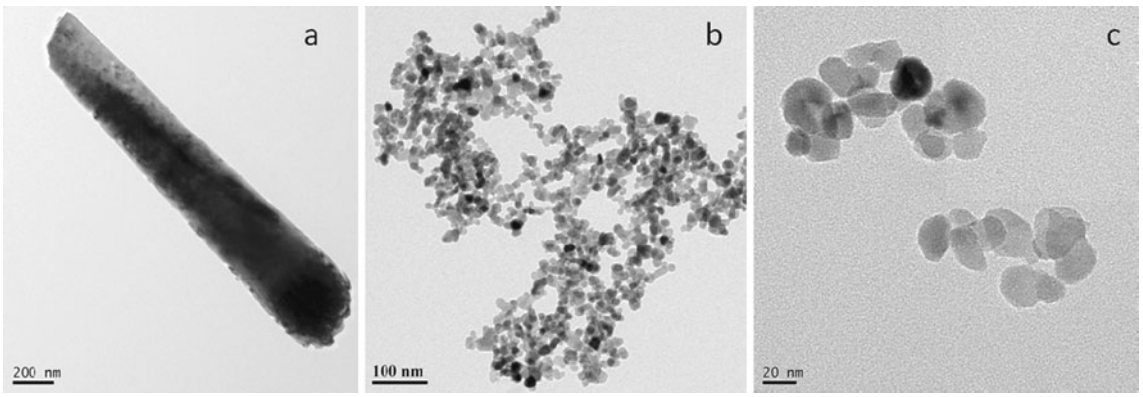

Fig. 4 HR–TEM image of **a** Z70-300, **b** ZRT-300 and **c** Pt/ZRT-300

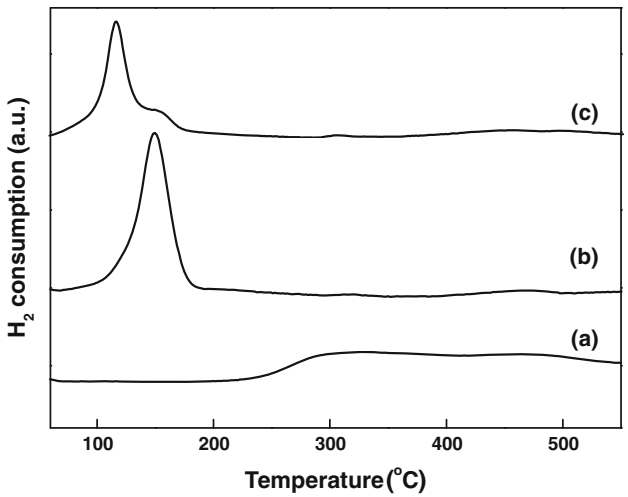

Fig. 5 TPR patterns (*a*) ZRT-300, (*b*) Pt/ZRT-300 and (*c*) Pt/Z70-300

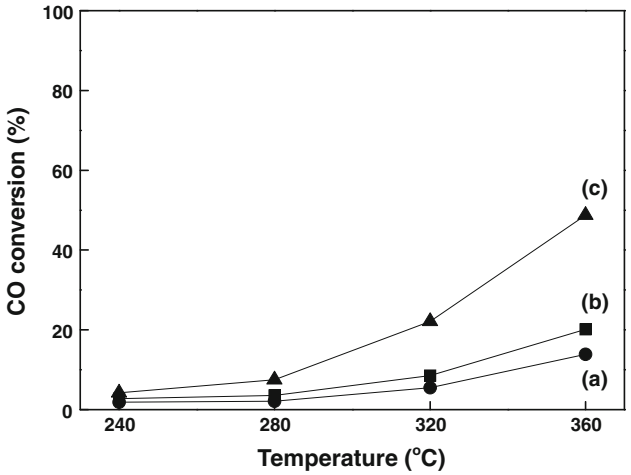

Fig. 6 CO conversion profiles over (*a*) Pt/Z70-300 and (*b*) Pt/ZRT-300 at the GHSV of 45,625 h^{-1} and (*c*) Pt/ZRT-300 at the GHSV of 13,652 h^{-1}

confirms that Pt/ZRT-300 has SMSI compared to Pt/Z70-300. As a result, it is expected that Pt/ZRT-300 catalyst will exhibit a high activity in WGS because this catalyst has oxidized Zn–PtO_x species with the SMSI, which are active species in WGS.

3.2 Reaction Results

The CO conversion profiles in WGS over the Pt/Z70-300 and Pt/ZRT-300 as a function of reaction temperature are shown in Fig. 6. For activity comparison, turn over frequency (TOF) value and reaction rate at 320 and 360 °C were calculated on both catalysts by carrying out the reaction at the GHSV of 45,625 h^{-1}. The values are

Table 1 TOFs and reaction rate results of Pt/ZRT-300 and Pt/Z70-300 catalysts

Catalyst	Temperature (°C)	Turnover frequency (s^{-1})	Reaction rate ($\mu mol_{CO}/g_{cat} \cdot s$)
Pt/ZRT-300	320	0.047	1.88
	360	0.112	4.44
Pt/Z70-300	320	0.032	1.22
	360	0.081	3.06

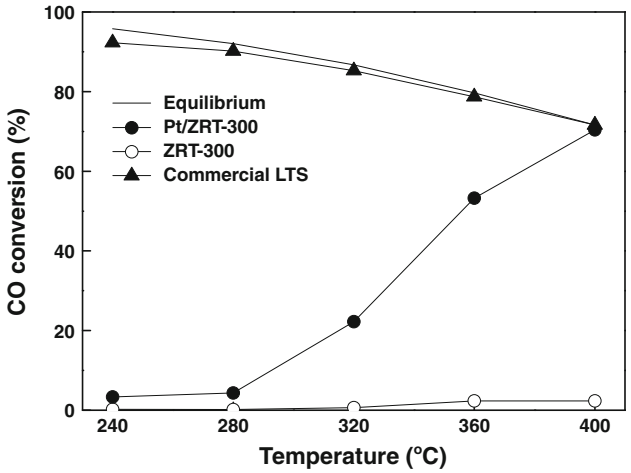

Fig. 7 CO conversion profiles over ZRT-300, Pt/ZRT-300, and commercial $Cu/ZnO/Al_2O_3$ catalysts ($H_2O/(CH_4 + CO + CO_2) = 2.0$; GHSV = 9,583 h^{-1})

compared and given in Table 1. It is obvious that Pt/ZRT-300 has higher TOF and reaction rate than Pt/Z70-300. This activity can be correlated to TPR results, which showed a weak metal support interaction for Pt/Z70-300 when compared to Pt/ZRT-300. Hence, further activity measurements were carried out at different GHSV on Pt/ZRT-300 to get the equilibrium conversion value of CO. When the GHSV is decreased from 45,625 to 13,652 h^{-1}, at 400 °C almost 20 % enhancement in the activity was observed as depicted in Fig. 6c.

At the GHSV value of 9,583 h^{-1} Pt/ZRT-300 catalyst exhibited almost equilibrium conversion value of 70 % at 400 °C as shown in Fig. 7. This indicates that this catalyst can be a potential candidate for medium temperature fuel cell applications. On the contrary, ZRT-300 showed almost negligible CO conversion at the same GHSV. These observations clearly demonstrate that the interaction of Pt with the nano-sized ZnO support generates active sites at the interface of the catalyst, which are useful for WGS. Hence, it is a bi-functional catalyst; in which both nano-sized Pt and ZnO support contribute to the activity for WGS. It is noteworthy that the activity of this catalyst was

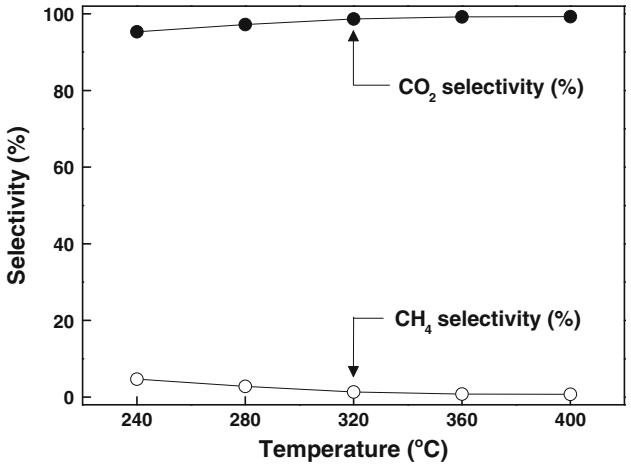

Fig. 8 Selectivity to CO_2 and CH_4 over Pt/ZRT-300 catalyst ($H_2O/(CH_4 + CO + CO_2) = 2.0$; GHSV = 9,583 h^{-1})

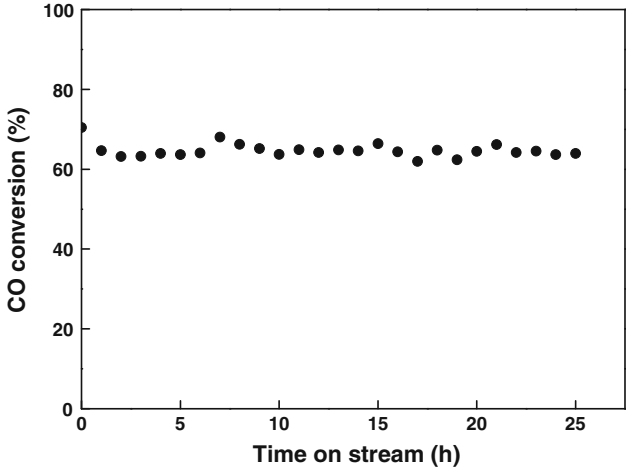

Fig. 9 CO conversion with time on stream ($T = 400$ °C) over Pt/ZRT-300 catalyst ($H_2O/(CH_4 + CO + CO_2) = 2.0$; GHSV = 9,583 h^{-1})

measured at the GHSV of 9,583 h^{-1}, which is 3.2 times higher than the typical GHSV (3,000 h^{-1}) in the industrial water gas shift reaction. As a reference catalyst, a commercial LTS catalyst, $Cu/ZnO/Al_2O_3$, was tested at the same condition. The LTS catalyst showed high conversion at the temperature above 240 °C. However, it is well known that Cu is susceptible to sintering at higher temperatures [56]. As a consequence, the LTS catalyst is not suitable for high temperature range.

Figure 8 depicts selectivity to CO_2 and CH_4 of this catalyst. At the reaction temperature of 200 °C, a methanation reaction occurred very slightly. On the contrary, almost 100 % selectivity to CO_2 was maintained above 250 °C. It was reported that Pt/ZnO has the ability to suppress the methanation reaction during WGS [57].

To check the stability of Pt/ZRT-300 catalyst in WGS reaction, CO conversion data with time on stream were collected at 400 °C for 25 h. Figure 9 shows the CO conversion data with time on stream. The CO conversion was slightly decreased at the initial stage. However, further significant deactivation was not detected for 25 h. This indicates that the stability of Pt/ZRT-300 appears promising. However, it is necessary to do long term tests along with start-up/shut-down cycling studies to evaluate the required stability.

All these above observations can be explained as follows. XRD, TPR, and H_2 chemisorption data indicate that the nano-sized Pt or Zn–PtO_x species are finely dispersed on the reducible nano-sized ZnO support due to a good interfacial contact between Pt and ZnO. In the nano-sized ZnO support, WGS can occur either through redox mechanism or through decomposition of associated intermediates. The nano-sized ZnO support is known to possess oxygen defects [58]. Then it is reasonable to expect that CO is oxidized into CO_2 at Pt metal interface by abstracting the oxygen from the ZnO lattice, resulting in its partial reduction. The oxygen defects will be simultaneously created within the ZnO lattice, which is refilled by the decomposition of H_2O at defect sites. The ZnO lattice is known to accommodate slightly excess zinc at the interstitial site within the structure. Moreover, H_2O always keeps oxidizing atmosphere and does not allow ZnO to get reduced to Zn metal particles or to form PtZn alloy at the surface in WGS. As a result, H_2O helps to maintain Pt in the form of Zn–PtO_x. Also as a partially reducible oxide, ZnO through the partial reduction can facilitate the dissociation of H_2O on the oxide surface, so that the formate species can be formed by the reaction of these special Type II bridging OH groups with CO [33]. The formates were known to be generated at lower temperatures since the partial reduction of the oxide was found to occur at lower temperature. In addition, the addition of noble metal can facilitate abstraction of hydrogen at the metal oxide interface, which in turn accelerates the formate decomposition rate [22, 23]. Hence, there would be an existence of analog for ZnO. The addition of Pt can promote the formate formation at low temperature, and also accelerate its decomposition. Thus, a dynamic equilibrium is quickly set up during the WGS.

4 Conclusion

1 wt% Pt/ZnO with rod-shape and spherical-shape were tested for WGS. The catalyst having spherical morphological feature showed higher TOF and reaction rate. The catalyst, Pt/ZRT-300 gave an almost equilibrium CO conversion value of 70 % at 400 °C, and 100 % selectivity to CO_2. No methanation activity was observed at the

reaction temperature above 250 °C. The high activity of this catalyst is mainly due to a good interfacial contact between Pt and ZnO.

Acknowledgments This Research was supported by a Basic Science Research Program through the National Research Foundation of Korea (NRF), funded by the Ministry of Education, Science and Technology (2010—0002521). This work was supported by the Korea Institute of Energy Research.

References

1. Carrette L, Friedrich KA, Stimming U (2001) Fuel Cells 1:5
2. Newsome DS (1980) Catal Rev 21:275
3. Cortright RD, Davda RR, Dumesic JA (2002) Nature 418:964
4. Ramachandran R, Menon RK (1998) Int J Hydrogen Energy 23:593
5. Suh DJ, Kwak C, Kim JH, Kwon SM, Park TJ (2005) J Power Sources 142:70
6. Song C (2002) Catal Today 77:17
7. Burch R (2006) Phys Chem Chem Phys 8:5483
8. Baronskaya NA, Minyukova TP, Khassin AA, Yurieva TM, Parmon VN (2010) Russ Chem Rev 79:1027
9. Schumacher N, Boisen A, Dahl S, Gokhale AA, Kandoi S, Grabow LC, Dumesic JA, Mavrikakis M, Chorkendorff I (2005) J Catal 229:265
10. Ratnasamy C, Wagner J (2009) Catal Rev 51:325
11. Ghenciu A (2002) Curr Opin Solid State Mater Sci 6:389
12. Ruettinger W, Ilinich O, Farrauto RJ (2003) J Power Sources 118:61
13. Qi X, Flytzani-Stephanopoulos M (2004) Ind Eng Chem Res 43:3055
14. Idakiev V, Tabakova T, Yuan ZY, Su BL (2004) Appl Catal A Gen 270:135
15. Jeong DW, Potdar HS, Roh HS (2012) Catal Lett 142:439
16. Fu Q, Saltsburg H, Flytzani-Stephanopoulos M (2003) Science 301:935
17. Duarte de Farias AM, Nguyen-Thanh D, Fraga MA (2010) Appl Catal B Environ 93:250
18. Vines F, Rodriguez JA, Liu P, Illas F (2008) J Catal 260:103
19. Zhai Y, Pierre D, Si R, Deng W, Ferrin P, Nilekar AU, Peng G, Herron JA, Bell DC, Saltsburg H, Mavrikakis M, Flytzani-Stephanopoulos M (2010) Science 329:1633
20. Pierre D, Deng W, Flytzani-Stephanopoulos M (2007) Top Catal 46:363
21. Schweitzer NM, Schaidle JA, Ezekoye OK, Pan X, Linic S, Thompson LT (2011) J Am Chem Soc 133:2378
22. Jacobs G, Graham UM, Chenu E, Patterson PM, Dozier A, Davis BH (2005) J Catal 229:499
23. Jacobs G, Williams L, Graham U, Thomas GA, Sparks DE, Davis BH (2003) App Catal A Gen 252:107
24. Pigos JM, Brooks CJ, Jacobs G, Davis BH (2007) Appl Catal A Gen 319:47
25. Pigos JM, Brooks CJ, Jacobs G, Davis BH (2007) Appl Catal A Gen 328:14
26. Liao F, Huang Y, Ge J, Zheng W, Tedsree K, Collier P, Hong X, Tsang SC (2011) Angew Chem Int Ed 50:2162
27. Wang YH, Zhu JL, Zhang JC, Song LF, Hu JY, Ong SL, Ng WJ (2006) J Power Sources 155:440
28. Chin YH, Dagle R, Hu J, Dohnalkova AC, Wang Y (2002) Catal Today 77:79
29. Guangwei X, Laitao L, Changquan L, Xiaomao Y (2009) Energy Fuels 23:1342
30. Ohta M, Ikeda Y, Igarashi A (2004) Appl Catal A Gen 258:153
31. Wang D, Ammari F, Touroude R, Su DS, Schlogl R (2009) Catal Today 147:224
32. Consonni M, Jokic D, Murzin DY, Touroude R (1999) J Catal 188:165
33. Shido T, Iwasawa Y (1991) J Catal 129:343
34. Kiennemann A, Chaumette P, Ernst B, Saussey J, Lavalley JC (1997) Stud Surf Sci Catal 107:55
35. Roh HS, Potdar HS, Jun KW, Han SY, Kim JW (2004) Catal Lett 93:203
36. Park JC, Bang JU, Lee J, Ko CH, Song H (2010) J Mater Chem 20:1239
37. Choi SO, Moon SH (2009) Catal Today 146:148
38. Roh HS, Jun KW, Dong WS, Chang JS, Park SE, Joe YI (2002) J Mol Catal A: Chem 181:137
39. Roh HS, Jun KW, Park SE (2003) Appl Catal A Gen 251:275
40. Oh YS, Roh HS, Jun KW, Baek YS (2003) Int J Hydrogen Energy 28:1387
41. Roh HS, Platon A, Wang Y, King DL (2006) Catal Lett 110:1
42. Roh HS, Wang Y, King DL (2008) Top Catal 49:32
43. Potdar HS, Jeong DW, Kim KS, Roh HS (2011) Catal Lett 141:1268
44. Jeong DW, Potdar HS, Kim KS, Roh HS (2011) Bull Kor Chem Soc 32:3557
45. Roh HS, Jeong DW, Kim KS, Eum IH, Koo KY, Yoon WL (2011) Catal Lett 141:95
46. JCPDS card No. 72-1100
47. JCPDS card No. 36-1451
48. Potdar HS, Roh HS, Jun KW, Ji M, Liu ZW (2002) Catal Lett 84:95
49. Matijevic E, Hsu WP (1987) J Colloid Interface Sci 118:506
50. Castellano M, Matijevic E (1989) Chem Mater 1:78
51. Ramos-Fernandez EV, Sepulveda-Escribano A, Rodriguez-Reinoso F (2008) Catal Commun 9:1243
52. Khan A, Smirniotis PG (2008) J. Mol Cat A Chem 280:43
53. Noei H, Qiu H, Wang Y, Loffler E, Woll C, Muhler M (2008) Phys Chem Chem Phys 10:7092
54. Hwang CP, Yeh CT (1996) J Mol Catal A: Chem 112:295
55. Navarro RM, Alvarez-Galvan MC, Sanchez–Sanchez MC, Rosa F, Fierro JLG (2005) Appl Catal B Environ 55:229
56. Twigg MV, Spencer MS (2001) Appl Catal A Gen 212:161
57. Korotkikh O, Ruettinger WF, Farrauto RJ (2003) Engelhard Corporation U.S. patent 6,562,315
58. Polarz S, Strunk J, Ischenko V, Van Den Berg MWE, Hinrichsen O, Muhler M, Driess M (2006) Angew Chem Int Ed 45:2965